USGS
science for a changing world

Geology and Geophysics Applied to Groundwater Hydrology at Fort Irwin, California

David C. Buesch, Editor

Airborne Electromagnetic Data and Processing within Leach Lake Basin, Fort Irwin, California

By Paul. A. Bedrosian, Lyndsay B. Ball, and Benjamin R. Bloss

Open-File Report 2013–1024–G

U.S. Department of the Interior
U.S. Geological Survey

U.S. Department of the Interior
SALLY JEWELL, Secretary

U.S. Geological Survey
Suzette M. Kimball, Acting Director

U.S. Geological Survey, Reston, Virginia: 2014

Suggested citation:
Bedrosian, P.A., Ball, L.B., and Bloss, B.R., 2014, Airborne electromagnetic data and processing within Leach Lake Basin, Fort Irwin, California, chap. G *of* Buesch, D.C., ed., Geology and geophysics applied to groundwater hydrology at Fort Irwin, California: U.S. Geological Survey Open File Report 2013–1024, 20 p., *http://dx.doi.org/10.3133/ofr20131024G*.

ISSN 2331-1258 (online)

Contents

Abstract 1
Introduction 1
Purpose and Scope 2
Geologic Background 3
Airborne Electromagnetic Survey 5
  Method and Measurements 5
  Data Preprocessing 7
Inversion of Electromagnetic Data 8
Model Assessment and Interpretation 10
  Igneous Framework 10
  Basin Fill 12
  Faulting 15
Geophysical Data Overview 17
  Flightlines 17
  Grids 17
  Line Data 18
  Plots 18
  Section Data 18
Acknowledgments 18
References Cited 19

Figures

1. Maps showing location of study area within Fort Irwin, California. 3
2. Photographs of the helicopter-borne AeroTEM IV system used during the airborne geophysical surveys in Leach Lake Basin, Fort Irwin, California. 6
3. Maps showing depth slices through the inverted resistivity model at a depth of *A*, 25 m and *B*, 125 m below land surface at Fort Irwin, California. 11
4. Example inverted resistivity section along flightline L10400. 13
5. Example inverted resistivity section along flightline L10880. 14
6. Map showing distribution of interpreted faults from airborne electromagnetic (AEM) models in relation to mapped faults in Leach Lake Basin, Fort Irwin, California. 16

Tables

1. Generalized sedimentary units within Leach Lake Basin, Fort Irwin, California. 4
2. System specifications for the airborne electromagnetic survey of Leach Lake Basin, Fort Irwin, California. . 7
3. Summary of EM1DINV inversion parameters used for final inversion of the airborne electromagnetic (AEM) data for Leach Lake Basin, Fort Irwin, California.. 9
4. Digital data organization and description for files and folders for the Leach Lake Basin study area, Fort Irwin, California. 17

Appendixes

[Available online only at http://pubs.usgs.gov/of/2013/1024/g/.]

- **A.** Report on a Helicopter-Borne AeroTEM System Electromagnetic & Magnetic Survey
- **B.** Airborne Magnetic and Electromagnetic Survey Data

Conversion Factors

SI to Inch/Pound

Multiply	By	To obtain
meter (m)	3.281	foot (ft)
kilometer (km)	0.6214	mile (mi)
square meter (m^2)	0.0002471	acre
square kilometer (km^2)	247.1	acre
nanotesla (nT)	1	gamma

Electrical conductivity is given in siemens per meter (S/m) unless otherwise specified.

Electrical resistivity is given in ohm-meters (ohm-m) unless otherwise specified.

Electrical resistivity (ρ, ohm-m) can be converted to conductivity (σ, S/m) as $\sigma = 1 / \rho$.

Datum

Vertical coordinate information is referenced to the North American Vertical Datum of 1988 (NAVD88).

Horizontal coordinate information is referenced to North American Datum of 1983 (NAD83), Universal Transverse Mercator projection, Zone 11 North (UTM11N).

Altitude, as used in this report, refers to distance above the vertical datum.

Acronyms

AEM	airborne electromagnetic
ECSZ	Eastern California Shear Zone
EM	electromagnetic
DOI	depth of investigation
DTM	digital terrain model
FEM	frequency-domain electromagnetic
GF	Garlock Fault
GPS	global positioning system
IGRF	International Geomagnetic Reference Field
LCI	laterally-constrained inversion
MSSP	Mojave strike-slip province
SAF	San Andreas Fault
TDS	total dissolved solids
TEM	time-domain electromagnetic
Tx	transmitter
USGS	U.S. Geological Survey

Abbreviations

A	Ampere
Hz	hertz
kHz	kilohertz
km	kilometer
m	meter
nT	nanotesla
$\Omega \cdot \mathrm{m}$	ohm-meter
ppm	parts per million
μs	microsecond
ms	millisecond
s	second
V	Volt

Airborne Electromagnetic Data and Processing within Leach Lake Basin, Fort Irwin, California

By Paul A. Bedrosian, Lyndsay B. Ball, and Benjamin R. Bloss

Abstract

From December 2010 to January 2011, the U.S. Geological Survey conducted airborne electromagnetic and magnetic surveys of Leach Lake Basin within the National Training Center, Fort Irwin, California. These data were collected to characterize the subsurface and provide information needed to understand and manage groundwater resources within Fort Irwin. A resistivity stratigraphy was developed using ground-based time-domain electromagnetic soundings together with laboratory resistivity measurements on hand samples and borehole geophysical logs from nearby basins. This report releases data associated with the airborne surveys, as well as resistivity cross-sections and depth slices derived from inversion of the airborne electromagnetic data. The resulting resistivity models confirm and add to the geologic framework, constrain the hydrostratigraphy and the depth to basement, and reveal the distribution of faults and folds within the basin.

Introduction

Groundwater flow in the arid basins of the Mojave Desert of the southwestern United States can be strongly influenced by faults. Effective conceptualization and modeling of these groundwater flow systems requires knowledge of the distribution and nature of hydrologically significant faults as well as the depth to basement rocks and general hydrostratigraphy. In an effort to understand, model, and manage groundwater resources in arid environments, the U.S. Geological Survey (USGS) is investigating Leach Lake Basin within the National Training Center, Fort Irwin, California (herein called Fort Irwin), using airborne and ground-based geophysical techniques. Toward this end, airborne magnetic and electromagnetic data were collected within Leach Lake Basin, a geologically complex, internally drained basin bisected and flanked by numerous Quaternary faults, including the Garlock Fault and the Southern Death Valley Fault Zone. Geophysical methods measure the variability in subsurface physical properties. In the case of airborne electromagnetic (AEM) methods, the derived property is electrical resistivity. This chapter presents the AEM data, while airborne magnetic data collected during this survey are discussed elsewhere (Langenheim and Jachens, this volume, chap. I).

Mapping subsurface geology and hydrostratigraphy in Fort Irwin is challenging. Given the complexity of the surface geology (Miller and others, this volume, chap. B), mapping subsurface structure and basin stratigraphy using direct-sampling techniques, such as drilling, is cost prohibitive and lends limited insight to the three-dimensional geometry of the subsurface structure. Logistical problems also exist: Leach Lake Basin is a year-round live-fire range, thus ground access is severly limited. Airborne geophysical methods provide an alternative to direct sampling and provide more spatially continuous data than ground-based surveys. Extensive faulting within the region means that these physical properties can vary substantially over short distances; thus, the dense spatial coverage

provided by airborne geophysical methods is critical to capturing abrupt changes in hydrostratigraphy and basement structure.

The AEM resistivity models provide subsurface constraints in excess of 200 m depth and show abrupt changes in earth response across faulted boundaries, reflecting the strong lateral resistivity contrast between igneous rocks and basin sediments. Intrabasin faults are identified, and, to a lesser extent, faults within the igneous basement can be traced. The distribution of faults throughout the basin can thus be directly obtained from the airborne data. The airborne resistivity models have additionally been used to trace hydrostratigraphy throughout the basin. Together with hydrologic investigations in neighboring basins, these results are being used to estimate groundwater storage within Leach Lake Basin.

Purpose and Scope

In December 2010 and January 2011, the U.S. Geological Survey conducted an airborne magnetic and airborne electromagnetic survey over Leach Lake Basin within Fort Irwin. Flightlines totaling 1,700 km were flown with 400-m nominal line spacing within a 46- by 16-km survey block (fig. 1). The eastern 10 km of the survey block was flown with 800-m line spacing. The majority of flightlines are oriented north-south; an additional three tie lines are oriented east-west and run along the northern and southern boundaries, as well as through the center, of the survey block. The AEM measurements were used to develop inverse models of the electrical resistivity structure along flightlines. The AEM resistivity models were combined into spatial grids which reveal the distribution of resistivity throughout the survey block. In conjunction with ground-based transient electromagnetic soundings, laboratory resistivity measurements on hand samples, and borehole geophysical logs from nearby basins, these models provide the basis for interpreting subsurface geology and show the distribution of faulting within Leach Lake Basin.

This report releases digital data from Leach Lake Basin. These data and the file structure are explained in the “Geophysical Data Overview” section. The methodology used to collect, process, and invert these data is presented in the “Airborne Electromagnetic Survey” section, and details of the inversion process are included in the “Inversion of Electromagnetic Data” section. A limited interpretation of the resulting inverse models is discussed in the “Model Assessment and Interpretation” section. A detailed interpretation is beyond the scope of this report.

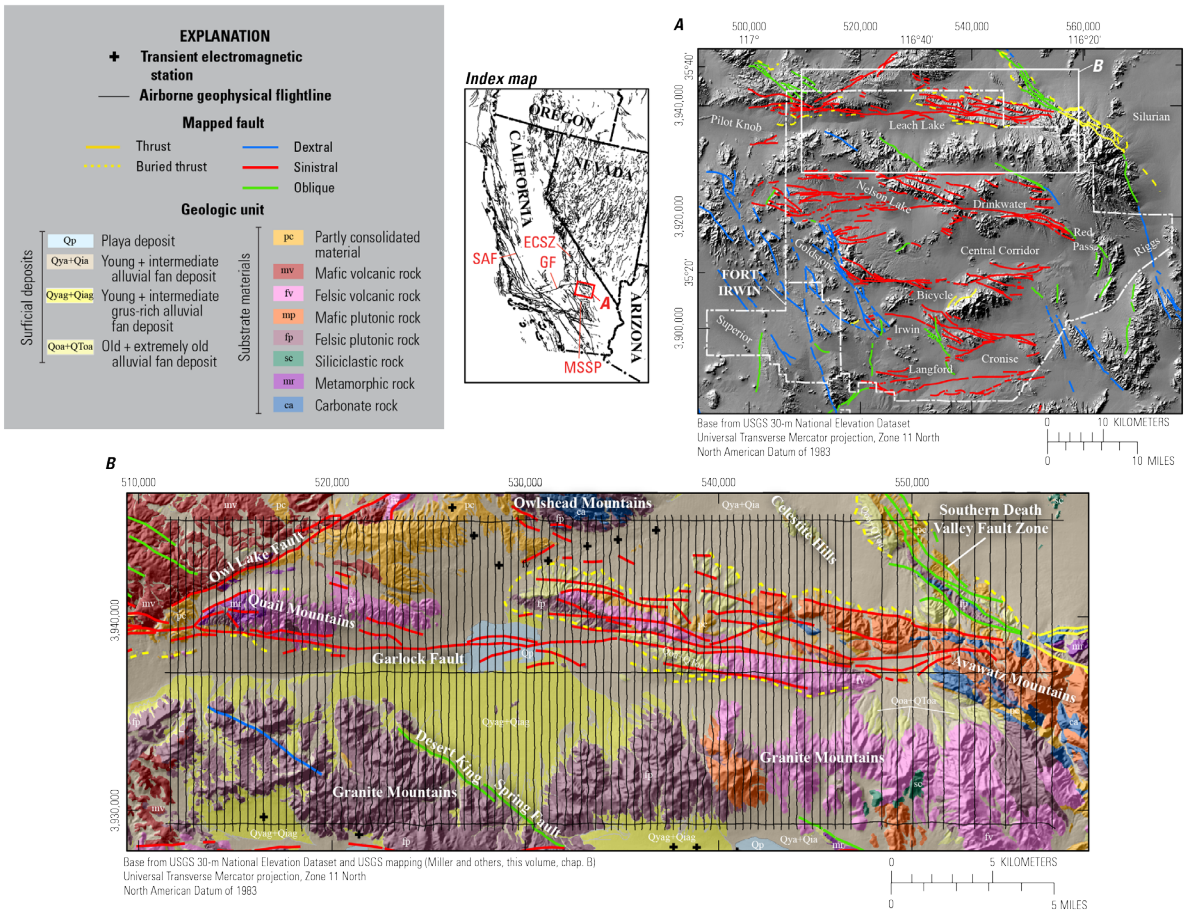

Figure 1. Maps showing location of study area within Fort Irwin, California. *A*, Fort Irwin boundary (dashed white line) with topographic basins labeled in white. Mapped faults are colored by sense of motion and illustrate east-west oriented sinistral faults (red), northwest-southeast oriented dextral faults (blue), and oblique faults (green). *B*, Leach Lake Basin study area with airborne electromagnetic (AEM) flightlines (black) and surface geology from Miller and others (this volume, chap. B). Black plus (+) symbols indicate locations of ground time-domain electromagnetic (TEM) soundings discussed in Burgess and Bedrosian (this volume, chap. F). Labeled faults on index map include Garlock Fault (GF), Mojave strike-slip province (MSSP), Eastern California Shear Zone (ECSZ), and San Andreas Fault (SAF).

Geologic Background

Fort Irwin, within the northeast part of the Mojave strike-slip province (Miller and Yount, 2002), accommodates late Cenozoic slip along the boundary of the North American and Pacific Plates east of the San Andreas Fault. This region consists of mountains separated by a series of topographic basins (fig. 1), all floored by mafic and felsic, volcanic and plutonic rocks. Precambrian basement and Paleozoic metasedimentary rocks are minor components, which were subsequently intruded by Jurassic and Cretaceous plutonic rocks (Miller and Sutter, 1982; Schermer and others, 1996). Deformation in the Middle Jurassic and again in the Early Cretaceous was deep seated and imprinted a mylonitic fabric

upon the older rocks (Schermer and others, 1996). A period of uplift and erosion occurred between Late Cretaceous plutonism and the onset of Miocene extension. Miocene and younger volcanism has further altered the landscape.

Tertiary and Quaternary sedimentary units (D. Buesch, written commun., 2014) deposited on this bedrock framework are described in table 1.

Table 1. Generalized sedimentary units within Leach Lake Basin, Fort Irwin, California.

Unit[1]	Description
pc	Moderate to weakly consolidated Tertiary deposits that may include volcanic or highly altered material. Includes silt and clay where weathered.
Qoa+QToa	Old alluvial fan deposits consisting of poorly sorted, compact to well-cemented sand and gravel that is less weathered than underlying units.
Qya+Qia	Young and intermediate alluvial fan deposits consisting of poorly sorted, compact to well-cemented sand and gravel that is less weathered than underlying units.
Qyag+Qiag	Young and intermediate grus-rich alluvial fan deposits consisting of unconsolidated sand and gravel. Formed mainly from grus derived from weathered granite.
Qp	Clay-rich playa deposits; typically at the center of many of the internally drained basins.

[1]Listed units are a subset of those found within Fort Irwin (shown in fig. 1*B)*.

Excluding clay-rich playa deposits (Qp), a general decrease in hydraulic conductivity with increasing depth is expected owing to sediment compaction and sealing of faults and fractures, although local variations in depositional environment (for example, provenance and grain size) are also expected to be reflected in the hydraulic properties of the sediments (Belcher and others, 2001). Where saturated, the older alluvial deposits (QToa) form the primary aquifer within basins of Fort Irwin; however, interbedded Miocene volcanics and sediments may also be an important source of water, as suggested by well production in Nelson Lake and Goldstone Lake Basins (D. Buesch, written commun., 2014).

The region is cut by numerous faults, including the dextral-oblique Southern Death Valley Fault Zone and the sinistral Garlock Fault; the latter is an important structure accommodating strain between the extensional tectonics of the Basin and Range province and right-lateral motion within the Mojave strike-slip province. These faults further reflect the two dominant styles of faulting within the region: (1) Cenozoic, sinistral, east-striking and (2) dextral, northwest-striking faults (fig. 1; Schermer and others, 1996; Miller and Yount, 2002). Additional details of the geology and faulting within the study area are described in Miller and others (this volume, chap. B).

Leach Lake Basin, the focus of the AEM survey, is a rhomb-shaped basin at the northern end of Fort Irwin that is bordered by the Owlshead and Granite Mountains to the north and south and the Quail and Avawatz Mountains to west and east (fig. 1). Over 1,000 m of relief separates the basin from the surrounding ranges. The ephemeral Leach Lake lies at the center of the basin and is bisected by the Garlock Fault, whose eastern terminus falls within the basin (fig. 1*B*).

Airborne Electromagnetic Survey

Method and Measurements

Within the brittle upper crust, electrical resistivity is sensitive to water content and quality, the presence of mineralogical clay, and changes in lithology. In the absence of clay or other conductive minerals, low electrical resistivity is typically associated with materials with high porosity, a high degree of saturation, or high total dissolved solid (TDS) levels in pore waters. In contrast, high electrical resistivity is related to low porosity, a low degree of saturation, and low TDS values. In sediments, resistivity also scales with grain size; the greater surface area associated with fine particles promotes the transmission of electrical current, in contrast to coarse-grained deposits, such as alluvial sand and gravel, which have relatively high bulk resistivity. Electrical resistivity is also highly sensitive to clay, small percentages of which can dramatically decrease bulk resistivity.

Helicopter-borne AEM systems transmit an electromagnetic signal from a towed air frame and induce current within the earth. The interaction of the earth with the induced current system gives rise to signals that are sensed by one or more receiver coils rigidly mounted to the air frame (fig. 2). Two basic types of AEM systems, both operating on the same physical principle, are commonly used for hydrogeophysical investigations. Frequency-domain electromagnetic (FEM) systems transmit a continuous sinusoidal current and measure the earth response in the on-time, while current is passing through the transmitter loop. Time-domain electromagnetic (TEM) systems transmit pulses of current and measure the earth response in the off-time, when no current is present in the transmitter loop. Geneally speaking, FEM systems have superior near-surface resolution, whereas TEM systems have a greater depth of investigation.

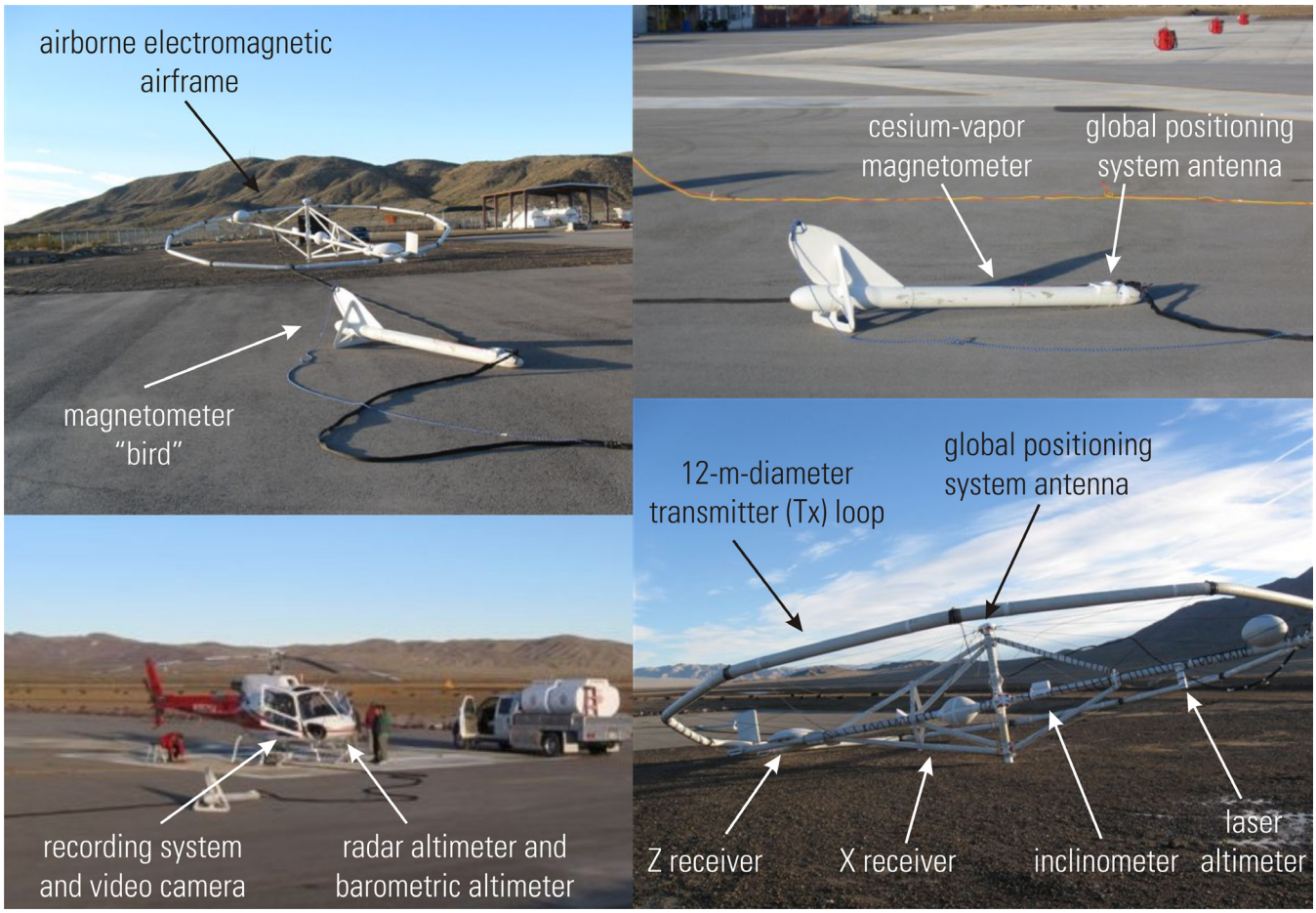

Figure 2. Photographs of the helicopter-borne AeroTEM IV system used during the airborne geophysical surveys in Leach Lake Basin, Fort Irwin, California. Electromagnetic sensors are affixed to a rigid, 12-m-diameter airframe that is flown at 50-m nominal height above land surface. Position, altitude, and attitude sensors are also affixed to the airframe. Magnetometer is attached to a "bird" that hangs along the tow line between the helicopter and the airframe.

For this study, the AeroTEM IV system was flown by Aeroquest, Ltd. Table 2 provides specifications of the system flown; a detailed description of data acquisition and contractor-performed processing are documented in the contractor's report (appendix A). Operationally, the AeroTEM IV system is analogous to ground-based TEM systems, the details of which are described by Burgess and Bedrosian (this volume, chap. F). A current is passed through a transmitter (Tx) loop, which sets up a primary magnetic field surrounding the loop. Upon shutting off current to the Tx loop, the collapsing magnetic field induces electrical currents in the subsurface. The interaction of these diffusing currents with the earth depends on subsurface resistivity structure and results in a secondary magnetic field measured at one or more loop receivers located inside of the Tx loop in the plane of the Tx (fig. 2).

When making TEM measurements from an airborne platform, the position, elevation, and attitude of the air frame must be accurately known. This ancillary information is obtained via additional sensors on the air frame, including a global positioning system (GPS) for positioning, a laser altimeter for elevation, and a three-component inclinometer for attitude. Principles of the TEM sounding method

can be found in Christiansen and others (2011), Fitterman and Labson (2005), Danielsen and others (2003), and Nabighian and Macnae (1991).

Table 2. System specifications for the airborne electromagnetic survey of Leach Lake Basin, Fort Irwin, California.

[The AeroTEM IV system was flown by Aeroquest, Ltd.]

Parameter	Setting
Frame type	Rigid frame
Receiver configuration	Central-loop
Waveform	Bipolar triangular
Base frequency	90 Hz
Measured time range	58 μs–3.2 ms
Transmitter loop turns	5
Peak current	397 A
Transmitter loop area	460 m^2
Transmitter moment	237,000 Am^2
Receiver altitude (mean)	48 m
Sounding spacing (mean)	3 m
Positioning (helicopter)	GPS
Positioning (airframe)	GPS
Elevation (helicopter)	Radar altimeter
Elevation (airframe)	Laser altimeter
Attitude (airframe)	Inclinometer

Data Processing

Airborne electromagnetic data, as delivered by airborne survey vendors, have typically undergone some degree of processing, most commonly filtering and leveling. The raw data stream (not provided by the contractor) consists of on- and off-time data from both X (along the flightline) and Z (vertical) receiver coils recorded at a 36-kHz sampling rate. The following data processing steps were carried out by Aeroquest Ltd. Data from 36 cycles, or transient decays, were stacked using a 50-percent overlapping straight stack. Stacked data were subsequently binned into gates of logarithmically increasing width using a boxcar window. A compensation procedure was then applied in which the effect of the residual primary Tx current was removed from the earliest measured time gates using data measured at high altitude (system response data), where the earth response is assumed to be zero. A gatewise linear drift correction was then applied between high-altitude system response measurements, which were carried out at the start and end of each flight. Filters applied to the data include a 19-point Hann window for smoothing and a single-point despiking filter to remove the effect of distant lightning.

Minimally processed data in appendix B incorporate the processing steps described above and these data were used in subsequent inversions. Data are additionally provided at three subsequent levels of contractor processing. Lag-corrected data are shifted in time relative to ancillary navigational data to account for a geometric offset between the electromagnetic sensors located on the air frame and navigational sensors on the helicopter and magnetometer bird. This correction was deemed unnecessary because additional position and altitude sensors were affixed to the air frame itself and are thus colocated with the electromagnetic sensors. Leveled and micro-leveled data have undergone varying degrees of tie-line leveling and decorrugation to produce smooth maps of the data at each time gate. Leveled data maps are of interest in qualitatively assessing the data and in searching for anomalous data responses. Leveling procedures, however, serve to reduce measured variations in signal amplitude

between lines that are associated with system height variations. As system height is modeled within the inversion procedure, leveled data, in which these variations are artificially muted, are unsuitable for inversion.

Inversion of Electromagnetic Data

The process of inversion is used to recover the distribution of resistivity with depth beneath each sounding. Inversion of AEM data is ill posed; that is, many resistivity models can fit the measured data, and the relationship between data and model is nonlinear. For this reason, regularization is needed to stabilize the inverse problem and to enforce specific properties in the inversion model such as proximity to a reference model or smoothness. Adjusting or determining the level of regularization is a critical part of any geophysical inverse problem and is intimately related to the spatial continuity of the problem, that is, how rapidly geologic structure and, by inference, resistivity structure vary both laterally and with depth. In smoothing regularization, too little regularization results in models that are patchy or discontinuous, whereas too much regularization gives rise to overly smooth models that do not capture the true degree of resistivity variation in the data. The effects of regularization on the inversion model are most pronounced at the greatest depths within the model section, where limited data bandwidth or low signal-to-noise levels limit the influence of the data in steering the inversion.

The determination of an appropriate level of regularization is inseparable from the specification of data errors. For AEM data, the difficulty lies in determining the data errors from the measured data, which, as typically delivered, have been filtered and smoothed, resulting in artificially small data errors. Additionally, the presence of systematic errors in the data can frustrate one's ability to accurately define data errors (Minsley and others, 2012). Most commonly, both data errors and the degree of regularization are adjusted during a series of trial inversions, with final parameters chosen that result in both a realistic model and an adequate fit to the measured data.

Assuming data errors are accurate and the degree of regularization is set appropriately, an inversion model section should reflect the true-earth model from the surface to the calculated depth of investigation (defined later in this section). We exploit this approach to define errors in the measured data. The southern part of the survey area (fig. 1*B*) consists of exposed Jurassic-Cretaceous granite, which is known to be resistive and is expected to extend to depths well beyond our depth of investigation. Data errors can be specified using a piecewise function that assigns the larger of 5 percent of the received signal or $\alpha \cdot t^{-1/2}$, where α is typically in the range of 10^{-11} to 10^{-14} $V/(m^2 \cdot s^{-1/2})$ and t is the time in seconds since the start of current turn-off. The form of this noise function reflects the $t^{-1/2}$ noise reduction associated with gate widths that increase logarithmically with time. Measured data over the granite were inverted from a moderately conductive starting model within a range of α values. Upon examining the resulting inverse models, a value of $\alpha = 1.3 \times 10^{-13}$ $V/(m^2 \cdot s^{-1/2})$ was found to produce a geologically realistic model: highly resistive from the surface to the maximum depth of investigation with no little or no indication of the conductive starting model within this interval.

An effort was made to exclude data from the inversion that show no appreciable earth response and are predominantly noise. This pertains mostly to late-time data, where signal-to-noise ratios are small, but entire soundings may effectively be noise in highly resistive areas. The contrast between resistive igneous basement rocks and conductive basin sediments results in highly variable signal levels and further demands a rigorous procedure to define the last usable time gate. An automated procedure was settled upon in which late-time data were excluded if dB_z/dt fell below 10^{-12} V/m^2 or if the curvature of a $\log_{10}(dB_z/dt)$ versus $\log_{10}(t)$ plot exceeded a threshold value of 10. Soundings were entirely omitted if early-time data fell below 10^{-10} V/m^2.

Having established the appropriate subset of data and estimated data errors, data at 16 time gates spanning an interval from 100 μs to 2.8 ms were inverted using the inversion code EM1DINV (Auken and Christiansen, 2004) coupled with the laterally-constrained inversion (LCI) approach of Auken and others (2005). Gate-center times are specified in the contractor's report (appendix A). The LCI approach links one-dimensional (1D) models at neighboring soundings together using regularization that enforces lateral continuity along a flightline. Data were decimated by a factor of 10 prior to inversion resulting in a 30-m nominal spacing between soundings. Blocks of 20 soundings (roughly 600-m line segments) were jointly inverted for linked 20-layer 1D models starting from a 100 Ω·m halfspace with no prior model enforced. The thickness of model layers varied from 8 m in the near surface to 42 m at depth with a total model depth of 380 m.

Vertical regularization, which effects how smoothly model resistivity varies with depth, was relaxed by a factor of 20 relative to lateral regularization. This ratio of vertical to lateral regularization reflects the expected high degree of lateral continuity within the basin sediments relative to abrupt changes in resistivity with depth, such as the sediment-basement contact. While this assumption appears to generally hold, the highly-faulted geologic setting is observed to produce abrupt lateral changes in received signal strength. To address such areas within the context of a laterally constrained inversion, the lateral regularization was locally relaxed in proximity to known or suspected structures using maxima in the along-profile gradient in dB_z/dt as a proxy for suspected faults or contacts. Table 3 provides a summary of the final inversion parameters applied to the Leach Lake Basin AEM data.

Table 3. Summary of EM1DINV inversion parameters used for final inversion of the airborne electromagnetic (AEM) data for Leach Lake Basin, Fort Irwin, California.

Parameter	Setting
Minimum/maximum gate centers	106 μs / 2.772 ms
Resistivity constraints	20
Thickness constraints	0.001 (fixed)
Vertical resistivity regularization	20
Vertical thickness regularization	0.001 (fixed)
Horizontal resistivity regularization	1
Horizontal thickness regularization	0.001 (fixed)
System altitude constraints	±3 m
Starting model	20 layers, 100 Ω·m, 380 m to top of half-space
Sounding exclusion threshold	dB_z/dt of first time gate less than 10^{-10} V/m^2
Data exclusion threshold	dB_z/dt at all time gates less than 10^{-12} V/m^2
Curvature cut-off criteria	All time gates beyond which curvature of $\log_{10}(dB_z/dt)$ versus $\log_{10}(t)$ exceeds 10 $V/(m \cdot s)^2$
Data errors	Greater of 5 percent dB_z/dt or $(1.3\times10^{-13})t^{-1/2}$ V/m^2
System bandwidth	70 kHz single-pole low-pass
Modeled current waveform	Bipolar triangular pulse

A TEM system must be properly characterized in order to recover realistic subsurface resistivity models (Christiansen and others, 2011). For both ground and airborne TEM systems, the frequency response of the system, the system geometry, and the current waveform must all be modeled accurately. For the AeroTEM IV system, the current waveform is known to vary during and between flights (both in timing and amplitude) and so is monitored by the contractor. We model a current waveform that varies dynamically throughout the survey area according to waveform parameters specified in appendix B. We further model two repetitions of the current waveform to account for the late-time effect of induction from earlier current pulses (Christiansen and others, 2011).

For the purpose of inversion, an accurate estimate of system height relative to land surface is also needed. Measurements of system height were obtained from the laser altimeter mounted on the air frame but were incorporated into the inversion with a standard error of 3 m. The inversion treats system height as a free parameter subject to the specified standard error. This approach, in which system height is allowed to vary relative to a measured starting value, accounts for inaccuracy in the measured system height associated with tilt of the air frame or canopy reflections. Topography is not explicitly incorporated within the inversion algorithm, however all inverse models have been hung on topography extracted from a 30-m resolution National Elevation Dataset grid.

Depth of investigation (DOI) is a valuable tool for evaluating the approximate depth in an inversion model to which data are sensitive. In the context of regularized inversion, the DOI helps discriminate between parts of the inverse model that are determined by the data and those that simply reflect the regularization applied to the inversion. We calculated a linear sensitivity-based DOI for each sounding, based upon the work of Christiansen and Auken (2010). In this approach, a columnwise sum of the Jacobian, or sensitivity matrix, is calculated for each layer resistivity within the model. The cumulative sum of the values for each layer resistivity, starting at the bottom of the model, is then used to estimate the DOI, assuming a threshold value of 0.8. This choice of threshold is subjective, and the DOI is best thought of as a relative, rather than absolute, indicator of the depth below which model resistivities are poorly constrained by the measured data.

The DOI is a very useful tool when displaying the final inversion model images because it provides a means for displaying areas of confidence in the model. A simple approach is to blank out regions of the model which fall below the DOI, preserving only those portions of the model that are well constrained by the measured data. This procedure has been applied to the inverted resistivity data provided in the SECTIONDATA folder under the ResINVDOI channel (appendix B).

Model Assessment and Interpretation

Igneous Framework

Examination of the resistivity model in map view (fig. 3) reveals strong resistivity contrasts within and surrounding Leach Lake Basin. The most resistive model features (>200 Ω·m) correspond to volcanic and plutonic rocks which floor and flank the basin. Mafic plutonic rocks, including diorite in the Avawatz Mountains (fig. 3, location 1a) and eastern Granite Mountains (fig. 3, location 1b), are extremely resistive (>1,000 Ω·m) and can be identified even in the measured data because received signal amplitudes plummet to the level of background noise. These regions can be identified on the model depth slices (fig. 3) as gaps in the resistivity grid.

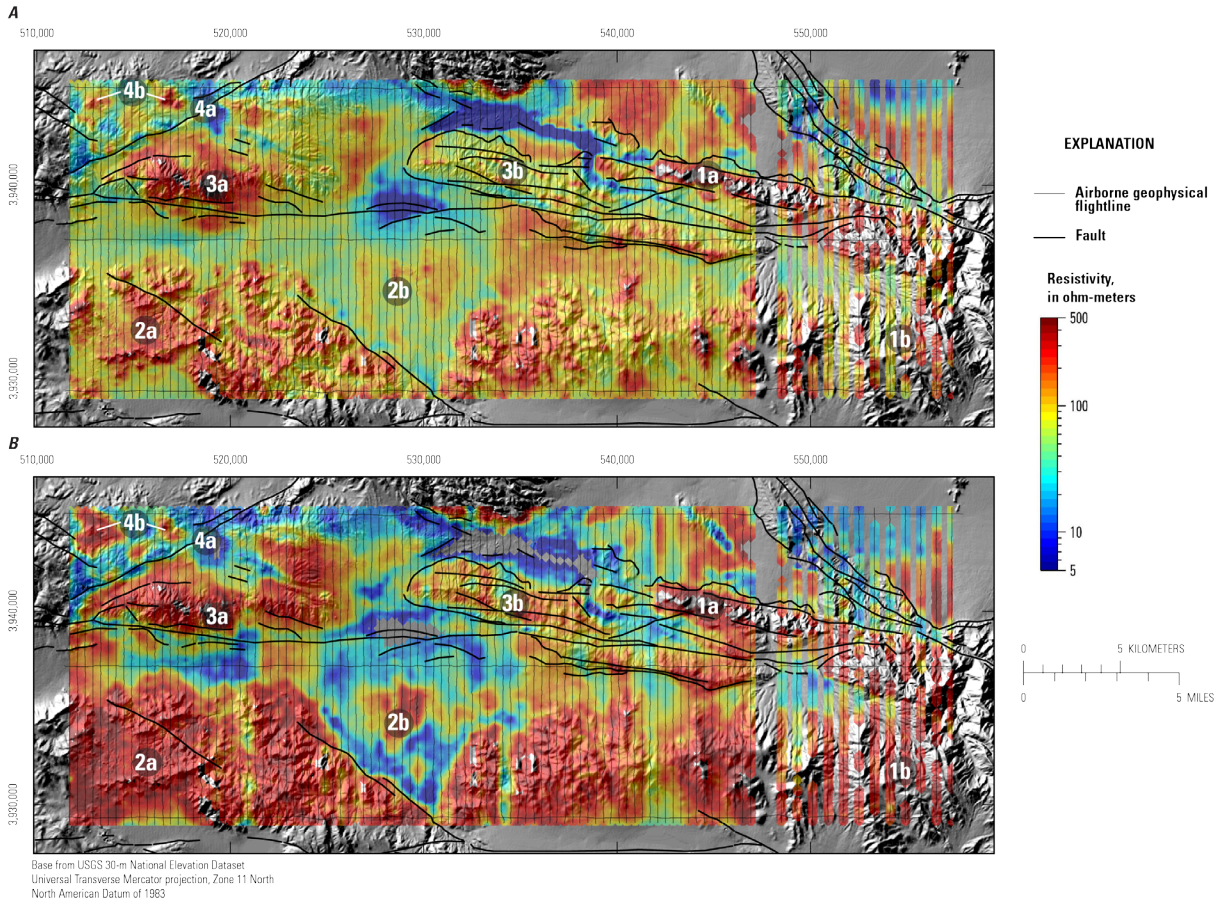

Figure 3. Maps showing depth slices through the inverted resistivity model at a depth of *A*, 25 m and *B*, 125 m below land surface at Fort Irwin, California. Labeled features are described in the text.

Granitic rock of the western Granite Mountains (fig. 3, location 2a) are generally resistive but in the near surface exhibit significant variability in resistivity over short distances. Upon close inspection, the spatial variability is closely correlated with exposed granitic ridges (resistive) and weathered depressions with localized sedimentary input (less resistive). This mottled appearance is a common geophysical expression of exposed intrusives and is evident in the magnetic field strength as well (Langenheim and Jachens, this volume, chap. I). Between Leach Lake and the Granite Mountains, shallow granite is imaged within the subsurface (fig. 3, location 2b) and is centered about small outcrops of granite within the basin fill (fig. 1*B*).

Felsic volcanic rocks in the Quail Mountains between the Garlock Fault and Owl Lake Fault (fig. 3, location 3a) exhibit similar resistivity values to the granite. Where mapped further east (fig. 3, location 3b), this rock unit has a more discontinuous resistive signature, possibly the result of dissection and translation along the Garlock Fault. Within the survey area, mafic volcanic rocks are mapped almost exclusively in the northwest corner of the survey area, are on average quite conductive (fig. 3, location 4a), and are juxtaposed against felsic volcanic rocks across Owl Lake Fault. The high conductivity of the mafic volcanic rocks in contrast to resistive felsic volcanic rocks may reflect a difference in the age

of emplacement or the degree of chemical or physical weathering. Two isolated resistive regions (fig. 3, location 4b) within the area of mapped mafic volcanic rock may be petrologically distinct from the surrounding material. This interpretation is further supported by color differences in Landsat imagery (fig. 4).

Basin Fill

The extent and shape of Leach Lake Basin, as well as the edges of surrounding basins, is clearly demarcated in map view by slices through the resistivity models (fig. 3) and by cross-sections along individual profiles (figs. 4, 5). Fault control on these tectonic basins is apparent by the sharp linear resistivity contrasts which bound the basin and in many cases correlate with mapped or inferred faults. A resistivity-based basin statigraphy can be derived from the AEM models. The extent and distribution of near-surface conductive deposits correlates with localized playa deposits (Qp) of Leach Lake (compare figs. 1 and 3). Basinwide, a change is typically observed between a thick package of moderately resistive (80–150 Ω·m) older alluvium (Qoa+QToa) and a thin surface veneer of young and intermediate age alluvium (Qya+Qia) (30–50 Ω·m) (fig. 4*B*). A subtle contrast in the resistivity of this surface veneer is sometimes observed between young alluvial fan deposits (Qya) in the northern half of the basin and grus-rich alluvial fan material (Qyag) in the southern half of the basin. This contrast is quite visible in Landsat imagery (fig. 4*A*). The most pronounced contrast, however, is between Qoa+QToa and underlying, highly conductive (<10 Ω·m) material (fig. 4*B*). This boundary can be traced throughout much of the basin. Significant topography on this interface (for example, fig. 5*B*) leads us to interpret this boundary as a lithologic change rather than a saturation boundary. This conclusion is supported by ground-based TEM models in Nelson Lake Basin, which show little correlation with water table elevations in nearby boreholes (Burgess and Bedrosian, this volume, chap. F) and further suggest the water table is not a significant resistivity boundary in this environment.

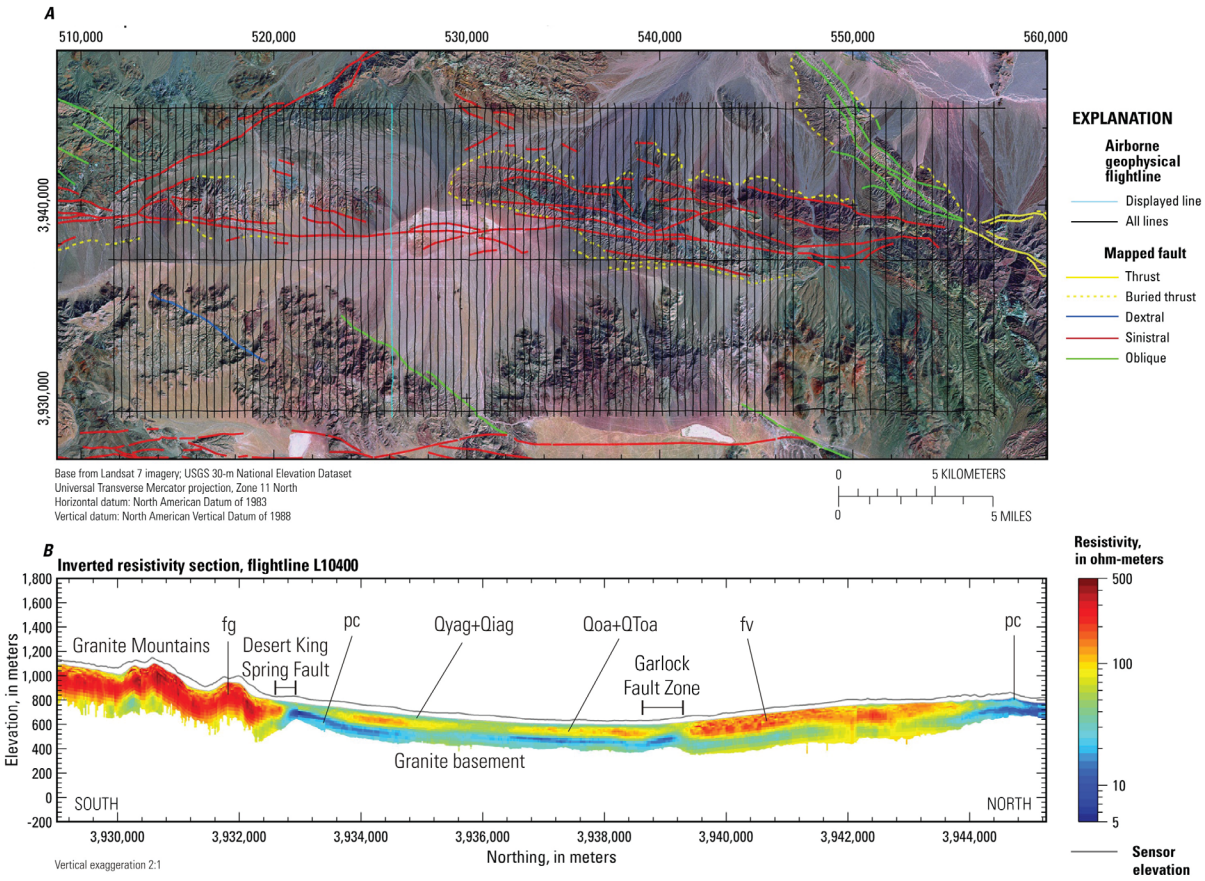

Figure 4. Example inverted resistivity section along flightline L10400. *A*, Index map with the location of flightline L10400 highlighted. *B*, Inverted resistivity model cross section along flightline L10400; vertical exaggeration 2:1.

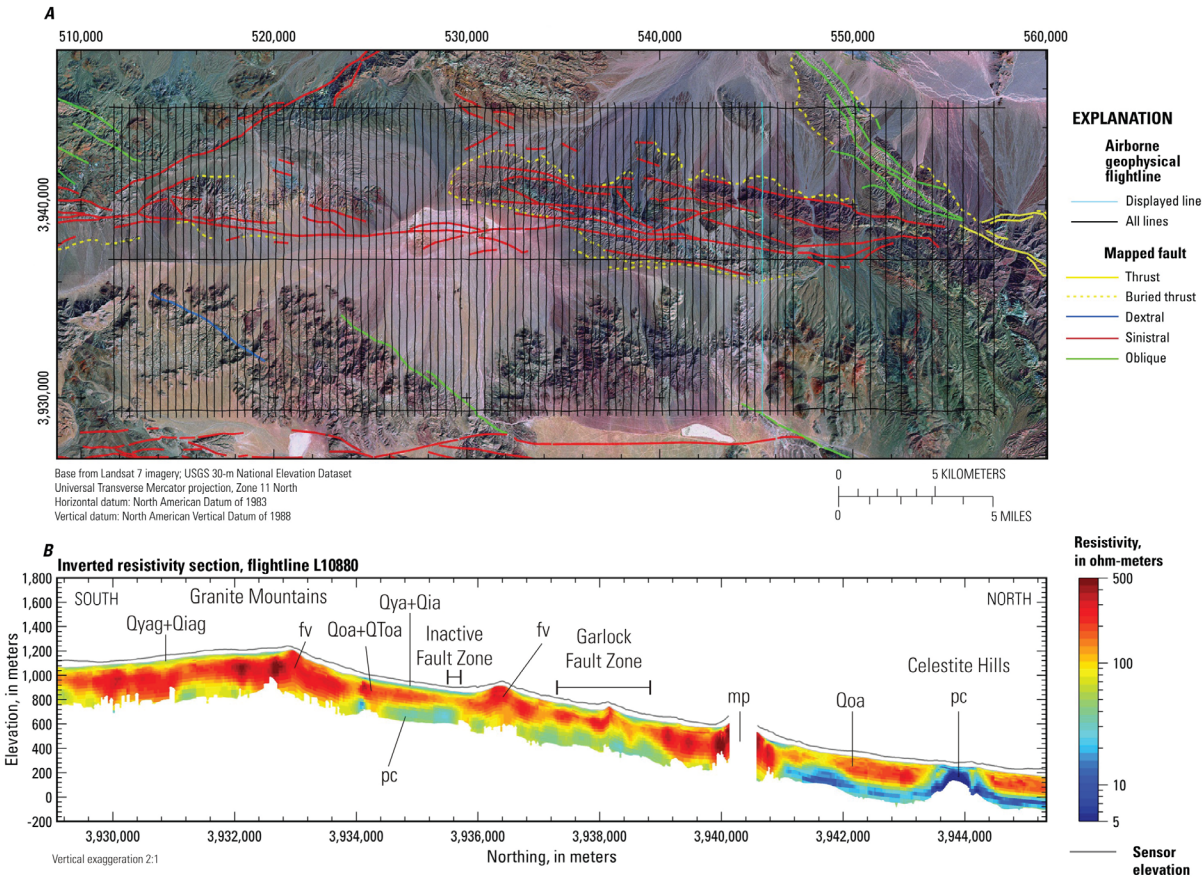

Figure 5. Example inverted resistivity section along flightline L10880. *A*, Index map with the location of flightline L10880 highlighted. *B*, Inverted resistivity model cross section along flightline L10880; vertical exaggeration 2:1.

The average depth to the top of the conductor is consistent with the average combined thickness of Qya+Qia (as much as 10 m) and Qoa+QToa (as much as 100 m) (Miller and others, this volume, chap. B). The base of this conductive unit is imaged within southcentral Leach Lake Basin, where it is inferred to rest directly on granite basement. Beyond Leach Lake Basin, this conductive stratum is imaged along the northern edge of Nelson Lake and Drinkwater Lake Basins and the western edge of southern Death Valley. The horizon is folded and faulted throughout the study area, suggesting significant tectonic movement syn- or postdeposition. As such, it may serve as an important tectonic marker in understanding the evolution of the region.

The highly conductive sediments are believed to reflect clay-rich, partially lithified sediments, probably Mio-Pliocene in age (fig. 1, map unit pc). These older sediments have limited surface exposure and are poorly understood; they have been mapped by several authors along the eastern boundary of Fort Irwin but may not be correlative even throughout this limited region (Brady and Troxel, 1999; Beratan and others, 1999; Sobieraj, 1994; Spencer, 1990). In other basins of Fort Irwin, ground-based TEM resistivity models image a similar conductive layer (<10 Ω·m) (Burgess and Bedrosian, this

volume, chap. B). In most cases, the conductor is at least 50–100 m below land surface, consistent with the limited exposure of map unit pc within Fort Irwin.

As part of an effort to identify the origin of the high conductivity sediments, laboratory resistivity measurements (Bloss and Bedrosian, this volume, chap. E) were carried out on hand samples of exposed sediments within Nelson Lake Basin and the Central Corridor that are thought to be older than map unit Qoa and possibly QToa. Laboratory measurements were also carried out on drill core samples within Nelson Lake Basin. Both the deepest drill core samples and the surface hand samples were found to be highly conductive (<10 Ω·m) when saturated to simulate conditions below the water table (Burgess and Bedrosian, this volume, chap. F). X-ray diffraction and X-ray fluorescence analyses were subsequently carried out on a subset of the drill core samples. The electrically conductive samples were found to have a high percentage of smectite clay as well as a large percentage of amorphous glass. The reaction of glass with water of moderate pH and low ionic strength is known to produce clay, predominantly smectite, as an alteration product (Vaniman, 2006). Miocene volcanism in the region is believed to be the source of the glass in the pre-Quaternary sediments. Some of this glass is interpreted to have been chemically weathered to smectite in the presence of water, giving rise to the high electrical conductivity. The Quaternary sediments, in contrast, contain less volcanic source material, have a low clay fraction, and are observed to be more resistive in laboratory measurements.

The AEM resistivity models suggest Leach Lake Basin is a relatively shallow basin. This finding is in agreement with gravity-derived depth-to-basement estimates (Jachens and Langenheim, this volume, chap. H). Both gravity and AEM methods suggest that the basin fill within Leach Lake Basin is no more than 200–300 m deep. Within the AEM survey area, the deepest sedimentary pile occurs outside of Leach Lake Basin along the west edge of the Southern Death Valley fault, where Qoa alone can exceed 300 m in thickess. This is again consistent with the gravity-derived depth-to-basement model; however, gravity coverage is very limited in this area. In Leach Lake Basin, three localized depocenters are identified on AEM models and confirmed by gravity models—in the west near the intersection of the Garlock and Desert King Spring Faults, near the dry Leach Lake bed, and in the east between the Garlock Fault and the eastern Granite Mountains. Quaternary sediments are interpreted to be thin or absent along an east-southeast striking corridor at the south edge of the Owlshead Mountains. Here, the conductive pc unit is imaged in the near surface and has been tightly folded and possibly faulted against the Owlshead Mountains.

Faulting

Understanding the geometry, extent, and activity of faults provides constraints on slip partitioning at the intersection between the Garlock and Southern Death Valley Fault Zones. The distribution of faults is also important when estimating groundwater storage because faults can reduce horizontal permeability and effectively compartmentalize groundwater into subbasins (see Burgess and Bedrosian, this volume, chap. F for a discussion of compartmentalization of groundwater in Nelson Lake Basin). The AEM resistivity models, both in map view and cross section, permit the direct identification of faults as abrupt, subvertical contrasts in resistivity. Basin-bounding faults, such as the Desert King Spring Fault, are most prominently imaged by the contrast between igneous basement and conductive sediments (fig. 4*B*). The top of conductive pc strata is often locally folded in the vicinity of such faults. Intrabasin faults, such as the Garlock Fault Zone, have a more subtle resistivity signature but can nevertheless be identified as disruptions in the otherwise flat-lying sedimentary strata (fig. 5*B*). In some cases, inactive fault strands can be inferred from the resistivity cross sections as continuous, flat-lying, near-surface sediments over discontinuous, older strata (for example, fig. 5*B*).

In map view, the broad pattern of faulting along the eastern terminus of the Garlock Fault Zone is evident (fig. 3). A series of east-southeast trending linear resistivity highs marks a series of positive flower structures in the basin sediments that diverge westward from the through-going Garlock Fault and may continue as far west as the Owl Lake Fault. Within the Avawatz Mountains, these push-ups incorporate slivers of basement rock, including felsic plutonic (fp), felsic volcanic (fv), and mafic plutonic (mp) rocks (fig. 1). The Southern Death Valley Fault Zone is imaged in cross section (not shown) as a set of tight folds that have been faulted and exhibit a clear southwest vergence, consistent with an oblique sense of slip. A similar structure is imaged in the Celestite Hills, southwest of the Southern Death Valley Fault Zone, albeit with no clear sense of vergence direction (fig. 5*B*).

In order to attain the distribution of faulting within the survey area, the resistivity cross sections were sequentially examined. Faults were inferred where abrupt lateral changes in resistivity or vertical offsets in subhorizontal layering were observed. The locations of faults inferred from the resitivity models are marked with circles on fig. 6. A remarkable correspondence is observed between faults identified from aerial photography and light detection and ranging (lidar) (C. Menges, unpub. data, 2012) and those independently identified from the AEM model (fig. 6). Major strands of the Garlock and Southern Death Valley Fault Zones are clearly identified from the AEM models, as are the Owl Lake and Desert King Spring Faults. In some cases, additional fault strands or previously unidentified faults are suggested by the AEM models (fig. 6, black dashed lines). These include northwest-striking faults between the Quail and Owlshead Mountains, a sub-parallel, older strand of the Garlock Fault at the northern edge of the Granite Mountains, and faulting in the Celestite Hills between the Southern Death Valley Fault Zone and the Garlock Fault Zone. Additionally, a series of northwest-striking linear features are suggested within the central and eastern Granite Mountains, in particular along their contact with basin sediments. These structures have an unusual orientation with respect to regional faulting (fig. 1) and may reflect local deformation associated with the termination of the Garlock Fault Zone within the Avawatz Mountains.

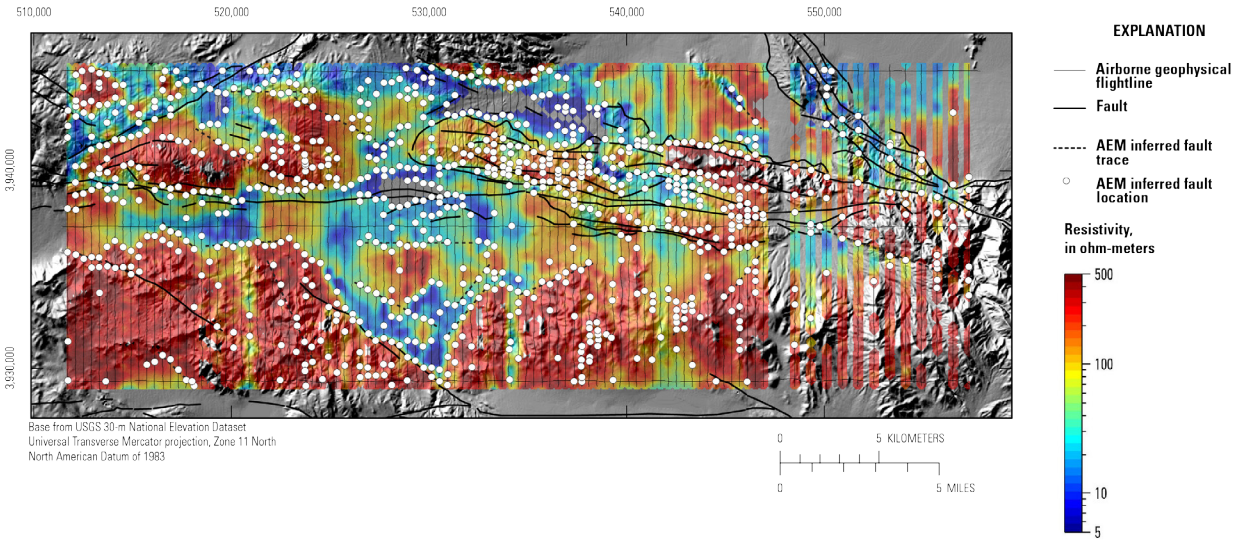

Figure 6. Map showing distribution of interpreted faults from airborne electromagnetic (AEM) models (white circles) in relation to mapped faults (solid black lines) in Leach Lake Basin, Fort Irwin, California. Dashed black lines indicate inferred fault traces or contacts. Background is a depth slice through the resistivity model at 125 m below land surface.

Geophysical Data Overview

Digital data are provided for the Leach Lake Basin survey area (see appendix B). Several products and data formats have been provided and are summarized in table 4 and described in the following sections in more detail.

Table 4. Digital data organization and description for files and folders for the Leach Lake Basin study area, Fort Irwin, California.

Folder	Description
FLIGHTLINE	Geospatial information consisting of survey flightlines (FLIGHT_LINES). Subfolders exist for AutoCAD files (LINE_DXF folder, *.dxf), shape files (LINE_SHP folder, *.shp), and keyhole markup language[1] (LINE_KML, *.kml) formats.
GRIDS	Gridded geophysical models created by the USGS. All grids are in Geosoft Oasis Montaj[2] format (GRID_GRD folder, *.grd), a standard of the geophysical industry used in many map display computer algorithms. Grids are also provided as georeferenced images in geoTIFF format (GRID_GEOTIFF folder, *.tif).
LINEDATA	AEM data in ASCII standard (*.xyz) and Geosoft Oasis montaj[2] (*.gdb) database formats. The README file in this directory contains channel heading descriptions.
PLOTS	Images of inverted resistivity sections (INVERTED_SECTIONS folder, *.pdf) and inverted model depth slices (INVERTED_SLICES folder, *.pdf).
SECTIONDATA	Databases of the inverted resistivity depth sections in ASCII standard (*.xyz) and Geosoft Oasis montaj[2] (*.gdb) database formats.

[1]Information on the keyhole markup language format and free GoogleEarth software can be found at http://www.google.com/earth/index.html.

[2]Information on the Oasis montaj program and a free data viewer can be found at http://www.geosoft.com/.

Flightlines

The FLIGHTLINE folder contains geospatial datasets of the flightline paths. The flightline location files are formatted in AutoCAD format (LINE_DXF folder, *.dxf), Esri Shapefile format (LINE_SHP folder, *.shp and associated files), and in GoogleEarth keyhole markup language format (LINE_KML folder, *.kml).

Grids

The GRIDS folder contains interpolated grids of various channels of the model section data from the Leach Lake Basin used to produce map plots. One of the challenges of gridding airborne geophysical data is that the spacing between flightlines (hundreds of meters or more) is much greater than the sampling down-line (a few meters). Gridding has been carried out using the minimum curvature method implemented by Webring (1981) for airborne geophysical data. This gridding method is implemented in Geosoft's Oasis montaj program (http://www.geosoft.com/resources/technology-papers/solution-earth-modeling). We have used this algorithm to produce 30-m-resolution grids of the inverted resistivity data from each model layer.

Grids are provided in two formats: Geosoft grid format (GRID_GRD folder, *.grd) and georeferenced geoTIFF images (GRID_TIFF folder, *.tif). The nomenclature for the grid names is given in the README file. The Geosoft grids can be viewed and analyzed in free software distributed by Geosoft (http://www.geosoft.com/support/downloads/viewers/oasis-montaj-viewer) or in various other mapping software packages using free plug-ins provided by Geosoft (http://www.geosoft.com/downloads). For example, the Geosoft-formatted grids can be viewed directly in the ESRI ArcMap application with the Geosoft ArcGIS plug-in (http://www.geosoft.com/support/downloads/plug-ins/plug-arcgis). Once the plug-in is installed and loaded in ArcMap, Geosoft grids can be handled within ArcMap in a similar manner to other types of raster data. GeoTIFF images can be viewed geospatially in most standard geographic information system software. The geoTIFF files can also be opened in several standard image-viewing software packages, including Windows Picture and Fax Viewer.

Line Data

The LINEDATA folder contains AEM survey data. The data are presented in Geosoft database format (*.gdb) and in ASCII format (*.XYZ contained within a *.zip file) with column headings as described in the README file. The contractor's report in appendix A also describes the digital flightline data.

Plots

The PLOTS folder contains plots of the inverted resistivity sections (INVERTED_SECTIONS folder, *.jpg) and depth slices (INVERTED_SLICES folder, *.pdf) for the Leach Lake Basin study area. Resistivity section plots have been generated for each flightline; the index map panel shows the location of the selected flightline being displayed in a given plot. Depth slices have been generated for the first 16 inversion model layers; the deepest three model layers fall largely below the estimated depth-of-investigation and are not provided in plots. All plots have been produced with a common color scale for all sections to allow comparison between flightlines.

Section Data

The SECTIONDATA folder containts the resistivity structure as a function of depth along the flightlines, as determined from the previously described inversion process. The DOI cutoff has been applied to the inverted resistivity values provided in the ResINVDOI channel. The depth intervals for each inversion model layer (DepTop and DepBot channels) are relative to land surface. Land-surface elevation along flightlines (NED30 channels) have been sampled from the 30-m resolution USGS National Elevation Dataset (http://ned.usgs.gov) and is specified in meters relative to the North American Vertical Datum of 1988 (NAVD88).

Acknowledgments

Airborne data collection was funded by the Fort Irwin National Training Center. The authors thank Aeroquest, Ltd. for their efforts in collecting this data set. In particular, we acknowledge the field crew (Lee Harper, Thomas Wade, and John Douglas) and the data processing team (Chris Kahue and Marion Bishop). We thank Jonathan Rudd for extended discussion and clarification of many aspects of the AeroTEM IV system and data processing. Matt Burgess, Sarah Falk, and Jill Densmore are thanked

for their help in acquiring ground-truth data for this survey. Bill Benzel is thanked for running X-ray diffraction and X-ray fluorescence analyses on drill core samples, the results of which informed our interpretation. Discussions with Chris Menges, David Miller, and David Buesch provided the geologic and tectonic context for these studies. John Dohrenwend processed the Landsat scenes to enhance features of geologic interest. Thanks to Ted Asch, Marya Deszcz-Pan, and Jeff Lucius for constructive reviews of this manuscript.

References Cited

Auken, E. and Christiansen, A.V., 2004, Layered and laterally constrained 2D inversion of resistivity data: Geophysics, v. 69, no. 3, p. 752–761.

Auken, E., Christiansen, A.V., Jacobsen, B.H., Foged, N., and Sørensen, K.I., 2005, Piecewise 1D laterally constrained inversion of resistivity data: Geophysical Prospecting, v. 53, no.4, p. 497–506.

Belcher, W.R., Elliot, P.E., and Geldon, A.L., 2001, Hydraulic-property estimates for use with a transient ground-water flow model of the Death Valley regional ground-water flow system, Nevada and California: U.S. Geological Survey Water-Resources Investigations Report 01–4120, 28 p.

Beratan, K.K., Hsieh, J., and Murray, B., 1999, Pliocene-Pleistocene stratigraphy and depositional environments, southern Confidence Hills, Death Valley, California, *in* Wright, L.A., and Troxel, B.W., eds., Cenozoic basins of the Death Valley region: Boulder, Colo., Geological Society of America Special Paper 333, p. 289–300.

Brady, R.H., III, and Troxel, B.W., 1999, The Miocene Military Canyon Formation; depocenter evolution and constraints on lateral faulting, southern Death Valley, California, *in* Wright, L.A., and Troxel, B.W., eds., Cenozoic basins of the Death Valley region: Boulder, Colo., Geological Society of America Special Paper 333, p. 277–288.

Burgess, M.K., and Bedrosian, P.A., 2014, Time-domain electromagnetic surveys at Fort Irwin, San Bernardino County, California, 2010–12, chap. F *of* Buesch, D.C., ed., Geology and geophysics applied to groundwater hydrology at Fort Irwin, California: U.S. Geological Survey Open File Report 2013–1024 (this volume).

Christiansen, A.V., and Auken, E., 2010, A global measure for depth of investigation in EM and DC modeling [abs.]: Australian Society of Exploration Geophysicists Extended Abstracts, vol. 2010, no. 1, 4 p.

Christiansen, A.V., Auken, E., and Viezzoli, A., 2011, Quantification of modeling errors in airborne TEM caused by inaccurate system description: Geophysics, v. 76, no. 1, p. F43–F52.

Danielsen, J.E., Auken, E., Jørgensen, F., Søndergaard, V., and Sørensen, K.I., 2003, The application of the transient electromagnetic method in hydrogeophysical surveys: Journal of Applied Geophysics, v. 53, no. 4, p. 181–198.

Fitterman, D. V., and Labson, V.F., 2005, Electromagnetic induction methods for environmental problems, *in* Butler, D.K. ed., Near-surface geophysics: Society of Exploration Geophysicists Books, Investigations in Geophysics series, no. 13, p. 301–355.

Jachens, R.C., and Langenheim, V.E., 2014, Gravity survey and interpretation of Fort Irwin and vicinity, Mojave Desert, California, chap. H *of* Buesch, D.C., ed., Geology and geophysics applied to groundwater hydrology at Fort Irwin, California: U.S. Geological Survey Open File Report 2013–1024 (this volume).

Langenheim, V.E., and Jachens, R.C., 2014, Aeromagnetic data, processing, and maps of Fort Irwin and vicinity, California, chap. I *of* Buesch, D.C., ed., Geology and geophysics applied to groundwater

hydrology at Fort Irwin, California: U.S. Geological Survey Open File Report 2013–1024 (this volume).
Miller, D.M., Menges, C.M., and Lidke, D.J., 2014, Generalized surficial geologic map of the Fort Irwin area, San Bernardino County, California, chap. B *of* Buesch, D.C., ed., Geology and geophysics applied to groundwater hydrology at Fort Irwin, California: U.S. Geological Survey Open File Report 2013–1024 (this volume).
Miller, D.M., and Yount, J.L., 2002, Late Cenozoic tectonic evolution of the north-central Mojave Desert inferred from fault history and physiographic evolution of the Fort Irwin area, California: Geological Society of America Memoir 195, p. 173–197.
Miller, E.L., and Sutter, J.F., 1982, Structural geology 40Ar-39Ar geochronology of the Goldstone-Lane Mountain area, Mojave Desert, California: Geological Society of America Bulletin, v. 93, no. 12, p. 1191–1207.
Minsley, B.J., Smith, B.D., Hammack, R., Sams, J.I., and Veloski, G., 2012, Calibration and filtering strategies for frequency domain electromagnetic data: Journal of Applied Geophysics, v. 80, p. 56–66.
Nabighian, M. N., and Macnae, J. C., 1991, Time-domain electromagnetic prospecting methods, *in* M.N. Nabighian, ed., Electromagnetic methods in applied geophysics: Society of Exploration Geophysicists Books, Investigations in Geophysics no. 3, v. 2, p. 427–520.
Schermer, E.R., Luyendyk, B.P., and Cisowski, S., 1996, Late Cenozoic structure and tectonics of the northern Mojave Desert: Tectonics, v. 15, no. 5, p. 905–932.
Sobieraj, J.A., 1994, Sedimentology and tectonics of Tertiary fan deposits, Fort Irwin, northern Mojave Desert, California: Bellingham, Wash., Western Washington University, M.S. thesis, 84 p.
Spencer, J.E., 1990, Late Cenozoic extensional and compressional tectonism in the southern and western Avawatz Mountains, southeastern California, *in* Wernicke, B.P., ed., Basin and Range extensional tectonics near the latitude of Las Vegas, Nevada: Boulder, Colo., Geological Society of America Memoir 176, p. 317–333.
Vaniman, David, 2006, Tuff mineralogy, chap. 2.2 *of* Heiken, G., ed., Tuffs—their properties, uses, hydrology, and resources: Geological Society of America Special Papers, v. 408, p. 11–15, doi: 10.1130/2006.2408(2.2).
Webring, M.W., 1981, MINC; a gridding program based on minimum curvature: U.S. Geological Survey Open-File Report 81–1224, 43 p.